doi:10.3788/gzxb20184702.0223001

基于四层等离子激元结构的椭球孔阵列光学漏波天线

钟东洲,刘程鹏
(五邑大学 信息与工程学院,广东 江门 529020)

摘 要:基于四层等离子激元结构(硅-金-硅-二氧化硅),通过在金属层中构造不同的椭球孔阵列,提出了两种不同结构的光学漏波天线,分别为一维对称锥形结构和二维对称锥形结构.基于天线理论和有限元方法,对天线的物理特性进行数值研究。研究结果表明:当工作波长为 1 550 nm 时,这两种光学漏波天线带宽都为 80 THz(包含了 S_+-L_+ 波段);当在天线端口处分别填充空气和氮化硅的时候,天线有较低的回波损耗和插入损耗,但对于两种不同的填充物,天线的特性表现出一些差异,例如,在一维对称结构中,天线端口处填充氮化硅时,天线有更少的回波损耗和插入损耗,更低的旁瓣电平,以及更好的方向性.该天线可用于光学集成互连、高度集成的光束控制和空间光通信中.

关键词:表面等离子激元;空间光通信;光学天线;有限元法;漏波天线;辐射方向图;天线阵列
中图分类号:O439 **文献标识码**:A **文章编号**:1004-4213(2018)02-0223001-10

Optical Leaky Wave Antenna with Ellipsoid Holes Array in Four-layer Plasmons Structure

ZHONG Dong-zhou, LIU Cheng-peng
(*School of Information Engineering, Wuyi University, Jiangmen, Guangdong* 529020, *China*)

Abstract: Based on the four-layer plasmons structure (silicon-metal-silicon-silica), two types of optical leaky-wave-antennas that have different ellipsoid-hole array structures in the metal layer were proposed. The structures include one-dimensional symmetric tapered array and two-dimensional symmetric tapered array. Based on antenna theory and finite element method, some physical characteristics for the antennas were investigated numerically. It is found that when the operating wavelength is fixed at 1550nm, the two antennas appear ultra wide bandwidth with 80 THz that covers the band of S_+-L_+. With their ports filled in the air and the silicon nitride, respectively, they both show low return loss and insertion loss. But for two types of different filled materials, their characteristics show some differences, for example, in a one-dimensional symmetric structure, the antenna has less return loss and insertion loss, lower side lobe level, and better directionality when its ports is filled with silicon nitride. The antenna can be generalized to apply in the fields of optical integrated interconnection, the control of highly integrated optical beam and space optical communication.

Key words: Plasmontic structure; Space optical communication; Optical antenna; Finite element method; Leaky-wave antenna; Radiation pattern; Antenna array
OCIS Codes: 230.3120; 240.6680; 350.4238; 130.3990; 160.4670; 350.3950

0 Introduction

Optical antennas have attracted considerable interest due to their applications ranging from the

Foundation item: National Natural Science Foundation of China (No. 61475120), Innovative Projects in Guangdong Colleges and Universities, China (No.2015KTSCX146)
First author: ZHONG Dong-zhou (1977—), male, professor, Ph.D. degree, mainly focuses on nonlinear and dynamic processes in semiconductor materials and lasers, nano-optoelectronic devices. Email: dream_yu2002@126.com
Received: Jun.21, 2017; **Accepted**: Nov.13, 2017

enhancement of absorption cross sections and quantum yields in photovoltaics [1-3], the release of energy efficiently from nanoscale light-emitting devices, the increase of spatial resolution in optical microscopy to space optical communication [4-6]. With the advent of nanoscience and nanotechnology, the fabrication of optical antenna structure is an emerging opportunity for novel optoelectronic devices[7]. By using surface plasmon theory and antenna theory, many researchers have been trying to develop new methods to analyze, explore [8-10] and design optical antennas [11-13]. The plasmon antennas proposed in [11-13] have been applied in spectropy[14], sensing [15], polarization manipulation [16], thin film lenses [17], manipulation of phase [18], photocatalysis [19] and so on. When the antennas are designed for space optical communication, many important parameters, such as return loss, insertion loss, side-lobe level, directivity, half power beam width, radiation pattern, bandwidth and so on, have to be considered. Motivated by these, several kinds of Optical Leaky Wave Antennas (OLWAs) applied in space optical communication have been proposed in some theoretical and experimental works. For example, Qi Song et al studied the optical leaky wave antenna consisting of a dielectric waveguide with periodic perturbation, and obtained a narrow beam radiation with a directivity of about 17.5dB [20]. In 2012, L.Yousefi and his coworkers proposed a novel patch nano optical antenna. Its structure is a mixing plasmon waveguide formed by wave impedance and working mode, but its gain and bandwidth are of 5.64dB and about 15THz, respectively [21]. To obtain better directionality, they designed a hybrid plasmon leaky wave antenna with the directivity of about 15.2 dBi [22]. In 2015, based on the cone algorithm, they put forward the hybrid plasmons leaky wave antennas with different waveguide structures, which have an ideal Sidelobe Level (SL) [23]. The antennas operating at a standard optical communication wavelength (1550nm) have good performances. For example, the directivity is 14.6dBi, the far-field radiation efficiency is 73% and the SL is -19.4dB, the bandwidth is 28THz that includes S and C bands for optical communications. In this paper, two new types of the OLWAs are proposed. They have different ellipsoid-hole array structures in the metal layer. Their physical properties, such as return loss, insertion loss, Radiation Pattern (RP), directivity, Half Power Beam Width (HPBW), SL and bandwidth, are further discussed in detail. The optical antennas presented in this paper exhibit better performances in bandwidth, SL level, return loss and insertion loss than those proposed so far by L. Yousefi and X. X. Liu [24-25].

1 One-dimensional symmetric tapered ellipsoid holes array

The structure ofthe OLWA is given in Fig.1. As shown in this diagram. Its spatial geometric structure has four layers such as silicon-gold-silicon-silica. In the gold layer, the ellipsoid holes are formed by the intersection of the cuboid and the ellipsoid. We taper the parameters of the ellipsoid holes and make their distribution to be One-Dimensional Symmetric Tapered Array (ODSTA), where the center of the symmetric is the middle position of the metal layer. The spacing d between each two adjacent ellipsoid holes is the period of the array, and fixed at 100nm. Using arithmetic progression, the main axes of the ellipsoid holes distributed in the left or the right side of the center of the metal layer are linearly decreased. As displayed in Fig.1, the main axis of the ellipsoid hole located at the central location is a_5 of 100 nm, but the main axes of those located in the right or left side of the center are in turn 90 nm, 80 nm, 70 nm and 60nm. The ellipsoid holes of 9 are filled with air. In additional, for any one ellipsoidal hole, the semi-minor axis $b=20$ nm; the semi-mean axis $c=30$ nm. In the four layers, the length of each layer material is the same. The length is defined as L_2 and set as 900 nm, SiO_2-material with low refractive index is placed in the bottom layer. Its height is 300 nm, defined as H_1. And its refractive index is set as 1.45. Si-material with high refractive index locates in the first-layer and third-layer, and its refractive index $n_{si}=3.5$. The height of the first layer and the third layer are defined as H_2 and H_4, respectively, which are fixed at 80 nm. The Au-material is sandwiched between two Si-material layers. Its height is named as H_3 and fixed at 20 nm. The width of the Air and Si_3N_4 in the OLWA are both 50 nm. The refractive index of the Si_3N_4 is 1.67. The total length of the antenna is defined as L_1 and set as 1 000 nm. The width of the antenna $W=200$ nm.

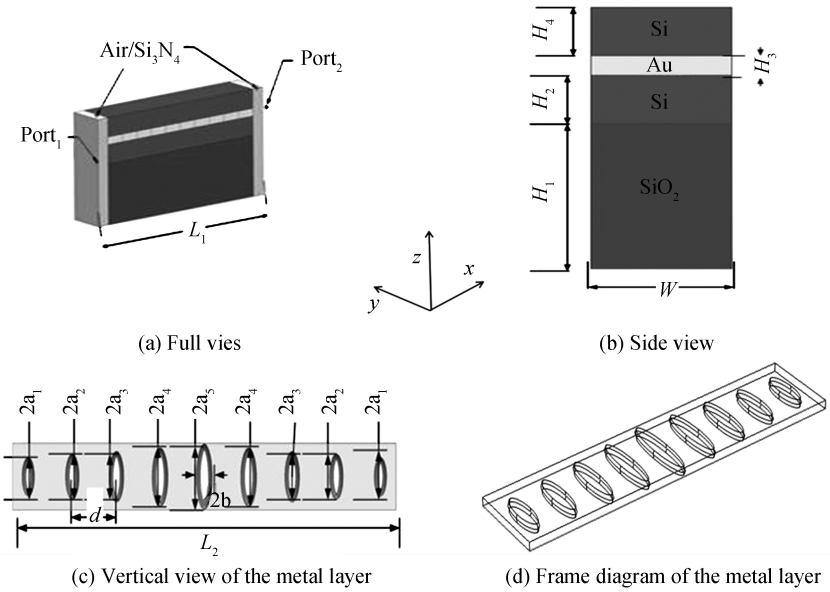

Fig.1 OLWA with one-dimensional symmetric tapered ellipsoid holes array in the metal layer

Moreover, for gold-material, the dielectric constant at high frequency is described by the revised of Drude model[26] as follows

$$\varepsilon(w)=\varepsilon_{\infty}-\frac{w_{\mathrm{p}}^{2}}{(w^{2}+\mathrm{i}\gamma w)} \tag{1}$$

Separating real and imaginary parts yields

$$\varepsilon_{\mathrm{re}}(w)=\varepsilon_{\infty}-\frac{w_{\mathrm{p}}^{2}}{(w^{2}+\gamma^{2})} \tag{2}$$

and

$$\varepsilon_{\mathrm{im}}(w)=\frac{\gamma w_{\mathrm{p}}^{2}}{w(w^{2}+\gamma^{2})} \tag{3}$$

where the plasma oscillation frequency W_{p} and the damping coefficient γ are given in [26], ε_{∞} is the instantaneous dielectric response.

1.1 Theory analysis

As shown in Fig. 1, the OLWA with ODSTA is designed based on the hybrid plasmonic structure[27]. These structures are developed by implementing a material with low refractive index (Au), between the two same materials with high refractive index (Si). This structure supports a guided plasmonic Transverse Magnetic (TM) mode, with high confinement inside the material with lower refractive index[27]. Since that the spacing d between each two adjacent ellipsoid holes is the same, and the distribution of the ellipsoid is periodical array, so the Au-layer is considered as a quasi-period structure. When the guided hybrid plasmatic mode enters to the optical antenna, it transforms to a radiating mode due to the quasi-periodic ellipsoid holes provided in the design. Since that the structure supports a TM plasmonic mode, the electric field has components both in the x, and z directions[28]. However, the z component is one order of magnitude bigger than the x component[29], due to the case that the big difference between the refractive index of the dielectric (Si) and that of the metal (Au). In this analysis, we can neglect the x component because that it is much smaller than z component, the z component of the electric field inside the optical antenna can be written in terms of a Fourier series expansion as[30]

$$E_{z}(y,x)=\sum_{m=-\infty}^{m=\infty}E_{m}(z)\,\mathrm{e}^{\mathrm{i}k_{x,m}x},k_{x,m}=k_{x,0}+\frac{2m\pi}{\mathrm{d}} \tag{4}$$

where d is the periodic, $k_{x,0}=\beta_{x,0}+\mathrm{i}\alpha$ is the wave number along the propagation direction, $\beta_{x,0}$ is a phase constant without the periodic disturbance, α is the attenuation constant. Before introducing periodic disturbance, the propagation constant of the initial mode is very close to the value of $\beta_{x,0}$, and the original attenuation constant in the antenna can be less than that of the α-parameter, due to the attenuation constant including only material loss and some scattering. On the contrary, due to the existence of

radiation, the value of the α-parameter increases significantly after introducing the periodic perturbation, $k_{x,m}$ is the Floquet wave numbers, m is the order of the Floquet space harmonic, $E_m(z)$ is the weight of the m-th harmonic. We obtain $k_{x,m}=\beta_{x,m}+\mathrm{i}\alpha$ since that $k_{x,0}=\beta_{x,0}+\mathrm{i}\alpha$, where$\beta_{x,m}=\beta_{x,0}+2\pi m/\mathrm{d}$ is the propagation constant of the m-th Floquet space harmonic. The periodic transverse ellipsoid apertures can generate radiation by the Floquet space harmonic, which can be controlled by the d-parameter. In these modes, compared with the number of waves in the vacuum, the modes with the smaller number are leaky mode and make the radiation beam

$$-k_0<\beta_{x,m}<k_0 \tag{5}$$

where,$k_0$is the wave number in vacuum; the OLWA is designed in such a way that above condition is satisfied with only for one Floquet mode ($m=-1$). So, only this mode generates the radiation beam, and other m-index Floquet modes are evanescent waves. From Eq. (5), it is found that the x-component of the electric field can be expressed as[31]

$$E(x)=E_{-1}\mathrm{e}^{\mathrm{i}\beta_{x,-1}x}\mathrm{e}^{-\alpha x}\ (0<x<L) \tag{6}$$

where $E_{-1}$is the amplitude of the harmonic electric field with the order of $m=-1$. In addition, for the OLWA, the main beam angle is related to the propagating mode wave number through[32]

$$k_{x,0}=\beta_{x,0}+\mathrm{i}\alpha \tag{7}$$

Therefore, the OLWA radiates light wave at broadside if $\beta_{x,-1}<<k_0$. The direction of the beam radiations orthogonal to the antenna when $\varphi=\pm\dfrac{\pi}{2}$. The far-field radiation pattern of the OLWA is obtained by integrating Eq. (7) as follows

$$E_{\mathrm{F}}=E_{-1}\frac{\mathrm{e}^{-\mathrm{i}(k_0\cos\varphi-\beta_{x,-1}-\mathrm{i}\alpha)L}-1}{-\mathrm{i}(k_0\cos\varphi-\beta_{x,-1}-\mathrm{i}\alpha)} \tag{8}$$

It is noted that the periodic disturbance of the OLWA is considered as the array of identical scatters. In this case, the scattered is derived from the far-field pattern. The pattern can be obtained by the multiplication of the normalized pattern of a single element and the normalized array factor $A_{\mathrm{F}}(\boldsymbol{\Phi})$, the total far-field radiation pattern is approximately represented by the $A_{\mathrm{F}}(\boldsymbol{\Phi})$ and expressed as

$$A_{\mathrm{F}}(\phi)=\frac{1-\mathrm{e}^{-\mathrm{i}(k_0\cos\varphi-\beta_{x,-1}-\mathrm{i}\alpha)Nd}}{1-\mathrm{e}^{-\mathrm{i}(k_0\cos\varphi-\beta_{x,-1}-\mathrm{i}\alpha)d}} \tag{9}$$

The antenna radiation power concentrated in the main lobeis often measured by the SL Level (SLL). The SLL is defined as the ratio of the peak of the SL and that of the Main Lobe (ML). The maximum SLL in the whole main pattern is defined as M_{SLL}. When it is expressed as a ratio in decibels (dB) [33]

$$M_{\mathrm{SLL}}(\mathrm{dB})=20\log_{10}\frac{|F_{\mathrm{SLL}}|}{|F_{\mathrm{MAX}}|} \tag{10}$$

where, F_{MAX} is the maximum amplitude of the pattern, F_{SLL} is the maximum amplitude of the highest SL. The directivity of the antenna is computed by using the following express [34]

$$D=\frac{4\pi}{\Omega_{\mathrm{A}}}\approx 4\pi\frac{(180/\pi)^2}{\theta_{1\mathrm{d}}\theta_{2\mathrm{d}}} \tag{11}$$

where, Ω_{A} is defined as the solid angle which all power would flow through if the antenna radiation intensity were constant at its maximal value. The beam solid angle can be approximated for antennas with one narrow main lobe and small sidelobe by simply multiplying HPBW in two vertical planes, $\theta_{1\mathrm{d}}$is the HPBW in one plane (in degrees) and $\theta_{2\mathrm{d}}$ is the HPBW in one plane at a right angle to the other (in degrees). According to the antenna theory, the Return Loss (RL) is the loss of power in the signal reflected by a discontinuity in an antenna. This discontinuity can be a mismatch with the terminating load. The RL is usually expressed as a ration in dB

$$\mathrm{RL}(\mathrm{dB})=10\log_{10}\frac{P_{\mathrm{i}}}{P_{\mathrm{r}}}=|\mathrm{S}_{11}|\ (\mathrm{dB}) \tag{12}$$

where, P_{i} is the incident power and P_{r} is the reflected power. Return loss is a measure of how well devices or lines are matched. A match is good if the return loss is high. The Insertion Loss (IL) is the loss of signal power resulting from the insertion of a device or antenna, which is given in dB by

$$\mathrm{IL}(\mathrm{dB})=10\log_{10}\frac{P_{\mathrm{T}}}{P_{\mathrm{R}}}=|\mathrm{S}_{21}|\ (\mathrm{dB}) \tag{13}$$

Where, P_T is the power transmitted to the antenna before insertion and P_R is the power received by the antenna after insertion.

1.2 Results and discussions

According to finite element method, it is necessary that the boundary conditions are set in the analysis of the OLWA structure. Here, we consider that the antenna is surrounded by spherical shells filled with air, which is set as perfectly matched layer boundary condition. The boundary condition is applied to implement absorbing boundaries. Based on this, we calculate the radiation patterns for TM wave in the OLWA with the ODSTA, where the ports filled with two types of materials such as air and Si_3N_4, as shown in Fig. 2. Here, to easily observe the HPBW at 3dB radiation patterns, the variation range of θ is enlarged from 0-2π to 0-4π. The HPBW in the xz plane, the yz plane and the xy plane are in turn defined as HPBW1, HPBW2 and HPBW3; the refractive index of Au-material is given in [35]; the operating wavelength of the OLWAS (λ) is fixed at 1550 nm. For the convenience of discussion, when air and Si_3N_4 are filled in the ports of the OLWA with ODSTA, respectively, the antenna is divided into two types. One is named as the ODSTA-air-OLWA for short, the other is called for short the ODSTA-Si_3N_4-OLWA. According to Eq. (11), the MSLL of the two OLWAs are calculated by using the radiation patterns in the xy plane, due to the fact that their SLs only exist in the xy plane (see Fig. 2). Thus, we obtain the MSLL of the ODSTA-air-OLWA and the ODSTA-Si_3N_4-OLWA as −4.8 dB and −5.5 dB, respectively. By carefully observing the radiation patterns in Fig. 2, we obtain the HPBWs in three planes for the two OLWAs, as displayed in Table 1. From Fig. 2(a), one further sees that θ_{1d} and θ_{2d} are of 90°(HPBW1) and 60°(HPBW3), respectively. So, the directivity D in the ODSTA-air-OLWA is obtained as 7.64 dBi from Eq. (9). Similar, the ODSTA-Si_3N_4-OLWAhas 9.44 dBi, where $\theta_{1d}=84°$ and $\theta_{2d}=52°$ [see Fig. 2 (b)]. The above results indicate that the ODSTA-Si_3N_4-OLWA has better direction and higher SLL than the ODSTA-air-OLWA.

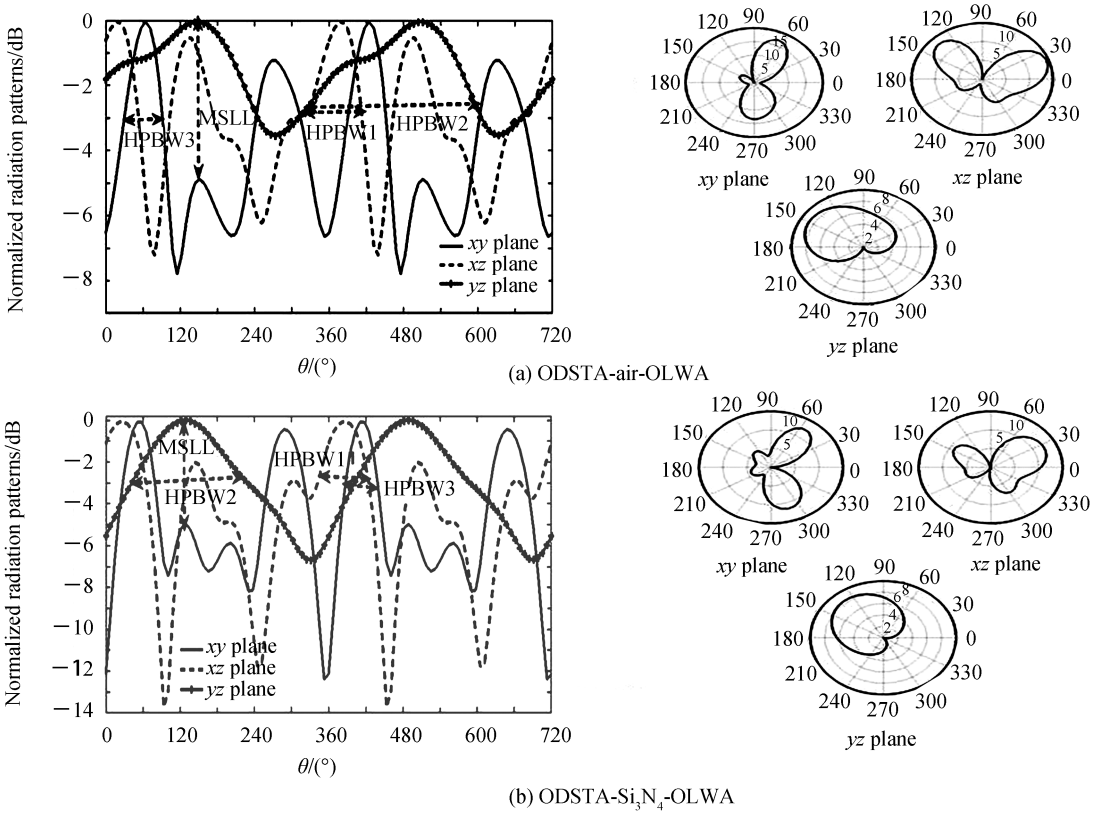

Fig.2 Normalized radiation patterns of the ODSTA-Si_3N_4-OLWA and the ODSTA-air-OLWA

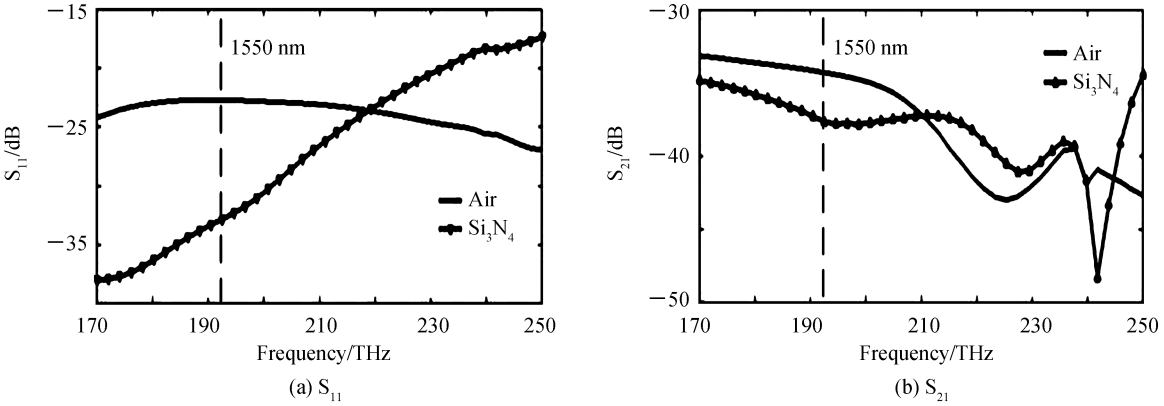

Fig.3 Plot of the S_{11} and the S_{21} versus the operating frequency in the OLWA with the ODSTA

Fig. 3 shows the dependence of S_{11} and S_{21} on the operating frequency of the OLWA with ODSTA when its ports are filled with air and Si_3N_4, respectively. As seen from Fig. 3, the operating bandwidth of the ODSTA-air-OLWA and the ODSTA-Si_3N_4-OLWA are in the whole frequency range (170～250THz), and the S_{21} of the two OLWAs are less than −32 dB. In the frequency range of 170～216THz, compared with the ODSTA-Si_3N_4-OLWA, there have the greater S_{11} and S_{21} in the ODSTA-air-OLWA. When λ is fixed at 1550 nm (the corresponding frequency is 193.5THz), for the ODSTA-air-OLWA, S_{11} and S_{21} are −22.3 dB and −34.5 dB, respectively; for the ODSTA-Si_3N_4- OLWA, S_{11} and S_{21} are −32 dB and −38 dB, respectively. The above discussions show that the ODSTA-Si_3N_4-OLWA has better matching than the ODSTA-air-OLWA.

2 Two-dimensional symmetric tapered ellipsoid holes array

Based on one-dimensional symmetric taperedarray ellipsoid holes, we prune further the metal layer structure of the OLWA, making it to become Two-Dimensional Symmetric Tapered ellipsoid holes Array (TDSTA) in the metal layer, as shown in Fig. 4. The parameters for the TDSTA are given as follows: W =430 nm, d_1 =230 nm. The other parameters are the same as those given in Fig. 1. For the sake of discussion, when the port of the OLWA with TDSTA is filled with air and Si_3N_4, it is divided into two types, named as the TDSTA-air-OLWA and the TDSTA-Si_3N_4-OLWA for short, respectively.

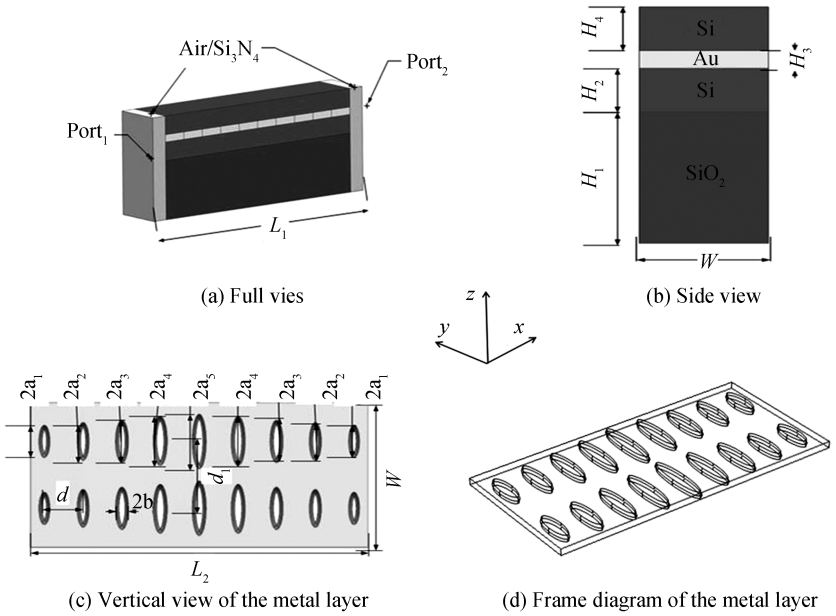

Fig.4 OLWA with two-dimensional symmetric tapered ellipsoid holes array in the metal layer

Fig. 5 gives the normalized radiation patterns of the OLWA with TDSTA in the metal layer at λ= 1 550 nm. As shown in Fig. 5, since that there appear only Back Lobes (BLs) in three planes of the TDSTA-air-OLWA or the TDSTA-Si_3N_4-OLWA, the BL Level (BLL) is used to measure the antenna

radiation power, and defined as

$$\mathrm{BLL(dB)}=20\log_{10}\frac{|F_{\mathrm{BLL}}|}{|F_{\mathrm{MAX}}|} \tag{14}$$

where, F_{BLL} is the maximum amplitude of the highest BL in three planes. By carefully observing Fig. 5, for the TDSTA-air-OLWA, BLL is obtained as −1.2 dB in the yz plane; but for the TDSTA-Si_3N_4-OLWA, it is −0.86 dB in the xz plane. In the two OLWAs, the HPBWs in the three planes are calculated and given in Table.1. It is further found from Fig.5 that $\theta_{1\mathrm{d}}$ and $\theta_{2\mathrm{d}}$ are 70° (HPBW1) and 105°(HPBW3), respectively. By calculating Eq. (9), we obtain the directivity D as 5.61dBi in the TDSTA-Si_3N_4-OLWA. Similar, D is 4.47 dBi in the TDSTA-air-OLWA, where $\theta_{1\mathrm{d}}=98°$ and $\theta_{2\mathrm{d}}=94°$. These results indicate that the TDSTA-air-OLWA has less BLL and better directivity than the TDSTA-Si_3N_4-OLWA.

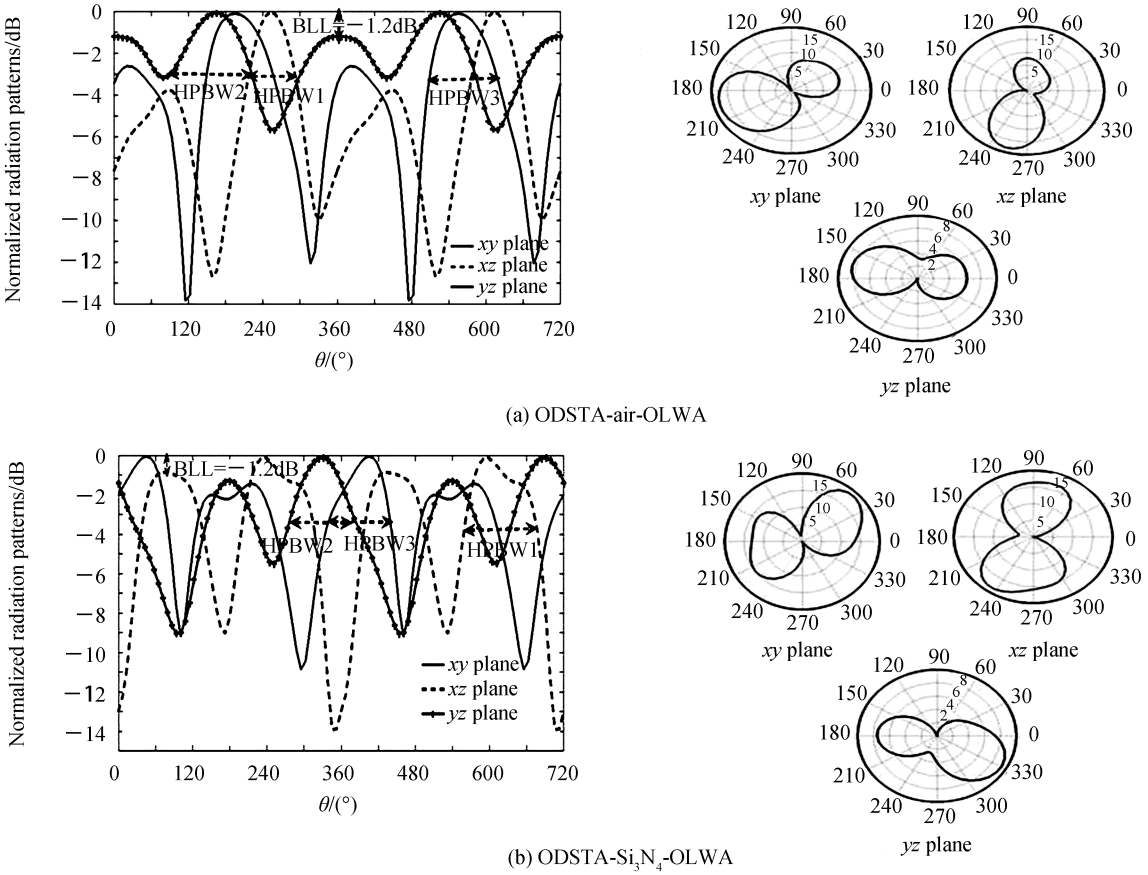

Fig.5 Normalized radiation patterns of the TDSTA-Si_3N_4-OLWA and the TDSTA-air-OLWA

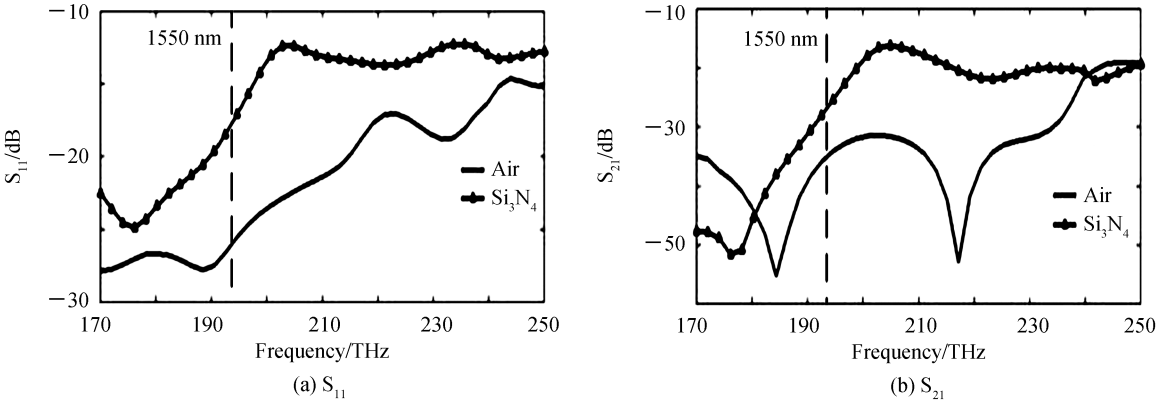

Fig.6 Plot of the S_{11} and the S_{21} versus the operating frequency in the OLWA with the TDSTA

Fig. 6 further displays the dependence of S_{11} and S_{21} on the operating frequency in the OLWA with the TDSTA, where the ports of the antenna are filled with air and Si_3N_4, respectively. From this diagram, it

is found that the TDSTA-air-OLWA has less S_{11} than the TDSTA-Si_3N_4-OLWA when the operating frequency ranges from 170 THz to 250 THz; the S_{21} of the TDSTA-air-OLWA is less than that of the TDSTA-Si_3N_4-OLWA if the operating frequency increases from 182 THz to 237 THz. For example, with λ fixed at 1 550 nm, in the TDSTA-air-OLWA, S_{11} is −26.5dB, but in the TDSTA-Si_3N_4-OLWA, it is −17.4 dB. In addition, the S_{21} of the TDSTA-air-OLWA and the TDSTA-Si_3N_4-OLWA are −35.5 dB and −27.2 dB, respectively, at λ=1 550 nm.

Table 1 presents the performance properties ofthe OLWAs with different gold layers and different mediums filled in the ports when λ=1 550 nm. From Table 1, it is concluded that the OLWAs with two different gold layers have wide bandwidth (80 THz) that covers the optical communication bands of S_+-L_+. There appear less scattering parameters (S_{11} and S_{21}), as well as better directivity in the OLWA with the ODSTA when its ports are filled with Si_3N_4. But for the OLWA with TDSTA, while its ports are filled with air, it exhibits less scattering parameters. It is noted that the OLWA with TDSTA has worse performance when compared with that with ODSTA in term of directivity. According to Eq. (11), the directivity depends on the HPBWs in two planes perpendicular to each other. It can be improved when the HPBWs are reduced by varying the parameters of the ellipsoid holes in the gold layer such as distance, main axes, semi axis.

Table 1 Performance properties of the OLWAs with different gold layers and different mediums filled in the portswhen the operating wavelength is fixed at 1 550 nm

Structure of ellipsoid holes in metal layer	Fillers	Band width/THz	S_{11}/dB	S_{21}/dB	HPBW1/(°)	HPBW2/(°)	HPBW3/(°)	D/dBi
One-dimensional symmetric tapered ellipsoid holes array	Air	80	−22.3	−34.5	90	285	60	7.64
	Si_3N_4	80	−32	−38	84	186	52	9.44
Two-dimensional symmetric tapered ellipsoid holes array	Air	80	−26.5	−35.5	70	132	105	5.61
	Si_3N_4	80	−17.4	−27.2	110	98	94	4.47

In order to verify the correctness of the calculation results, Fig. 7 gives the comparison of the S_{11} and that of the S_{21} in the ODSTA with the ports filled with air, obtained by COMSOL and FDTD software. Similar, the comparison of the S_{11} and that of the S_{21} in the TDSTA with the ports filled with air are displayed in Fig. 8. From Figs. 7 and 8, it is found that the dependence of the S_{11} on the operating frequency obtained by COMSOL is similar to that computed by FDTD. Also, the plot of the S_{21} versus the operating frequency by using COMSOL is very close to that by using FDTD. These shows that the calculation results are verified to be correct.

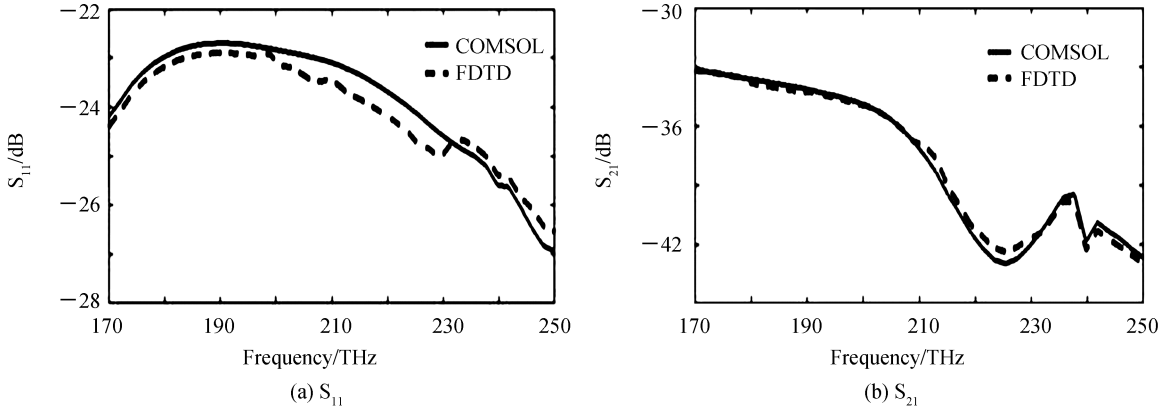

Fig.7 Comparison of the S_{11} and that of the S_{21} in the OLWA with the ODSTA

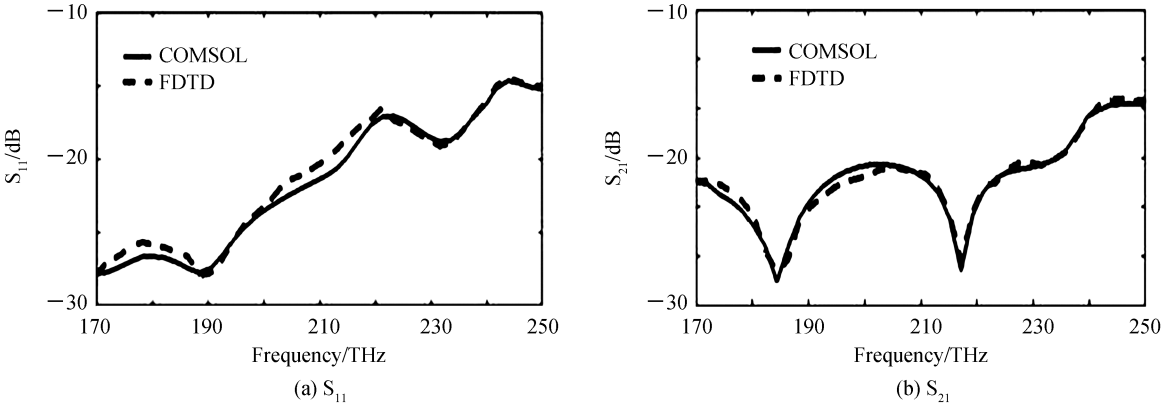

Fig.8 Comparison of the S_{11} and that of the S_{21} in the OLWA with the TDSTA

3 Conclusion

In this paper, to achieve good matching, super wide bandwidth, good directivity, high SLL or BLL, we propose the optical leaky wave antenna with four layers waveguide structure such as silicon-gold-silicon-silica. In the gold layer, two types of ellipsoid-hole arrays, such as one-dimensional symmetric tapered array, two-dimensional symmetric tapered one, are formed in the gold layer. The OLWAs with different gold layers exhibit ultra wide bandwidth (80THz) that covers most of the optical communication bands of $S_+ \sim L_+$. Also, they show great difference in radiation pattern. For one-dimensional symmetric tapered array of ellipsoid holes, the SL of the antenna only exists in the xy plane of the radiation pattern. But for two-dimensional symmetric tapered array, there is no SL in the radiation pattern. For each type of ellipsoid array, the antenna has different performances in SLL or BLL, return loss, insertion loss, HPBW and directivity when its ports are filled with air and Si_3N_4, respectively. For example, the OLWA with one-dimensional symmetric tapered array has less return loss and insertion loss, and lower SLL, as well as better directivity while its ports are filled with Si_3N_4. In additional, the less return loss, the less insertion loss and lower BLL will occur in the OLWA with two-dimensional symmetric tapered array if air is filled in the ports. The OLWA with good performance properties proposed in this paper can be generalized to apply in the fields of optical integrated interconnection, the control of highly integrated optical beam, space optical communication and so on.

References

[1] SPADACCINIC M, HOPKINS J B, SHAW L A. Scanning holographic optical tweezers [J]. *Optics Letters*, 2017, **42**(15):2862-2865.

[2] YANG T, MA L, GAO Z,*et al*. Two-dimensional hetero structure as a platform for surface-enhanced Raman scattering [J]. *Nano Letters*, 2017, **17**(4):2621-2626.

[3] YIFAT Y, ACKERMAN M, GUYOTSIONNEST P. Mid-IR colloidal quantum dot detectors enhanced by optical nano-antennas [J]. *Applied Physics Letters*, 2017, **110**(4):041106-041109.

[4] YANG Tian, TATSUMA T. Mechanisms and applications of plasmon-induced charge separation at TiO_2 films loaded with gold nanoparticles [J]. *Journal of the American Chemical Society*, 2005, **127**(20): 7632-7637.

[5] VIETZ C, KAMINSKA I, SANZ P M, *et al*. Broadband fluorescence enhancement with self-assembled silver nanoparticle optical antennas [J]. *Acs Nano*, 2017, **11**(5): 4969-4975.

[6] WENZEL M T, HARTLING T, OLK P, *et al*. Gold nanoparticle tips for optical field confinement in infrared scattering near-field optical microscopy [J]. *Optics Express*, 2008, **16**(16): 12302-12312

[7] BURKE P J, LI S, YU Z. Quantitative theory of nanowire and nanotube antenna performance [J]. *IEEE Transactions on Nanotechnology*, 2004, **5**(4): 314-334.

[8] YIFAT Y, EITAN M, ILUZ Z, *et al*. Highly efficient and broadband wide-angle holography using patch-dipole nanoantenna reflect arrays [J]. *Nano Letters*, 2014, **14**(5): 2485-2490.

[9] YIFAT Y, ILUZ Z, BAR-LEV D, *et al*. High load sensitivity in wideband infrared dual-Vivaldi nanoantennas [J]. *Optics Letters*, 2013, **38**(2): 205-207.

[10] REN X, SHAS Wei, CHOY W. Tuning optical responses of metallic dipole nanoantenna using grapheme [J]. *Optics Express*, 2013, **21**(26): 31824-31829.

[11] CHEN K, RAZINSKAS G, FEICHTNER T, *et al*. Electromechanically tunable suspended optical nanoantenna. [J].

Nano Letters, 2016, **16**(4):2680-2685.
[12] ZHU Lu, WANG Yang, LIU Yuan-yuan, *et al*. The design of the slot yagi nano-antenna and the absorption characteristics of wide band [J]. *Acta Photonica Sinica*, 2016, **45**(10): 138-145.
[13] BUTET J, THYAGARAJAN K, MARTIN O J. Ultrasensitive optical shape characterization of gold nanoantennas using second harmonic generation [J]. *Nano Letters*, 2013, **13**(4): 1787-1792.
[14] APPAVOO K, LEI D Y, SONNEFRAUD Y, *et al*. Role of defects in the phase transition of VO2 nanoparticles probed by plasmon resonance spectroscopy [J]. *Nano Letters*, 2012, **12**(2): 780.
[15] ZHANG W, MARTIN OJF. A universal law for plasmon resonance shift in biosensing [J]. *Acs Photonics*, 2014, 2(1): 144-150.
[16] PETSCHULAT J, CIALLA D, JANUNTS N, *et al*. Doubly resonant optical nanoantenna arrays for polarization resolved [J]. *Optics Express*, 2010, **18**(5): 4184-4197.
[17] TVINGSTEDT K, DAL Z S, INGANASI O, *et al*. Trapping light with micro lenses in thin film organic photovoltaic cells [J]. *Optics Express*, 2008, **16**(26): 21608-21515.
[18] KATS M A, BLANCHARD R, GENEVET P, *et al*. Thermal tuning of mid-infrared plasmonic antenna arrays using a phase change material [J]. *Optics Letters*, 2013, **38**(3): 368-370.
[19] SALMISTRARO M, SCHWARTZBERG A, BAO W, *et al*. Triggering and monitoring plasmon - enhanced reactions by optical nanoantennas coupled to photocatalytic beads [J]. *Small*, 2013, **9**(19):3301-3307.
[20] SONG Q, CAMPIONE S, BOYRAZ O, *et al*. Silicon-based optical leaky wave antenna with narrow beam radiation [J]. *Optics Express*, 2011, **19**(9): 8735-8749.
[21] YOUSEFI L, FOSTER A C. Waveguide-fed optical hybrid plasmonic patch nano-antenna [J]. *Optics Express*, 2012, **20**(16): 18326-18335.
[22] YOUSEFI L. Highly directive hybrid plasmonic leaky wave optical nano-antenna [J]. *Progress in Electromagnetics Research Letters*, 2014, **50**: 85-90.
[23] PANAHI M A, YOUSEFI L, SHAHABADI M. Highly directive hybrid plasmonic leaky-wave optical antenna with controlled side-lobe level [J]. *Journal of Lightwave Technology*, 2015, **33**(23): 4791-4798.
[24] SACHER W D, HUANG Y, DING L, *et al*. Wide bandwidth and high coupling efficiency Si_3N_4-on-SOI dual-level grating coupler [J]. *Optics Express*, 2014, **22**(9): 10938-10947.
[25] LIU X X, ALU A. Subwavelength leaky-wave optical nanoantennas: Directive radiation from linear arrays of plasmonic nanoparticles [J]. *Physical Review B Condensed Matter*, 2010, **82**(14): 2635-2645.
[26] LAKOWICZ J R. Radiative decay engineering: biophysical and biomedical applications [J]. *Analytical Biochemistry*, 2001, **298**(1): 1-24.
[27] SALVADOR R, MARTINEZ A, *et al*. Analysis of hybrid dielectric plasmonic waveguides [J]. *IEEE Journal of Selected Topics in Quantum Electronics*, 2008, **14**(6): 1496-1501.
[28] PITARKE J M, SILKIN V M, CHULKOV E V, *et al*. Theory of surface plasmons and surface-plasmon polaritons[J]. *Reports on Progress in Physics*, 2006, **70**(1): 1-87.
[29] YOUSEFI L, FOSTER A C. Waveguide-fed optical hybrid plasmonic patch nano-antenna [J]. *Optics Express*, 2012, **20**(16): 18326-18335.
[30] JACKSON D R, OLINER A A. Leaky - wave antennas [M]. Modern Antenna Handbook. John Wiley and Sons, Inc, 2007: 325-367.
[31] COLLIN R E. Antennas and radiowave propagation [M].Antennas and radiowave propagation. McGraw-Hill, 1985:79-116.
[32] BALANIS C A. Antenna theory: analysis and design, 3rd edition [M]. Wiley, 2012.
[33] CROSWELL W. Antenna theory, analysis, and design [M]. Harper and Row, 1982.
[34] BALANISC A. Antenna theory and design [M]. John Willey and Sons, Inc, 2005.
[35] JOHNSON P B. Optical constants of the noble metals [J]. *Physical Review B*, 1972, **6**(12): 4370-4379.